IRIS AperTO

UNIVERSITÀ DEGLI STUDI DI TORINO

AperTO - Archivio Istituzionale Open Access dell'Università di Torino

Computational approach to the study of epitaxy: natural occurrence in diamond/olivine and aragonite/zabuyelite.

This is the author's manuscript

Original Citation:

Availability:

This version is available http://hdl.handle.net/2318/1520349 since 2016-06-21T11:54:02Z

Published version:

DOI:10.1021/acs.cgd.5b00389

Terms of use:

Open Access

Anyone can freely access the full text of works made available as "Open Access". Works made available under a Creative Commons license can be used according to the terms and conditions of said license. Use of all other works requires consent of the right holder (author or publisher) if not exempted from copyright protection by the applicable law.

(Article begins on next page)

13 May 2024

A computational approach to the study of epitaxy: the natural occurrence in diamond/forsterite and aragonite/zabuyelite

Marco BRUNO,*[†] Marco RUBBO,[†] Linda PASTERO,[†] Francesco Roberto MASSARO,[†] Fabrizio NESTOLA,[‡] Dino AQUILANO[†]

[†]Dipartimento di Scienze della Terra, Università degli Studi di Torino, Via Valperga Caluso 35, I-10125, Torino Italy.

[‡] Dipartimento di Geoscienze, Università degli Studi di Padova, Via Gradenigo 6, I-35131, Padova Italy

*Corresponding author
e-mail: marco.bruno@unito.it
Tel. +390116705126
Fax: +390116705128

Abstract

In this contribution the theoretical and computational aspects related to the determinations of the (i) interface structure, (ii) adhesion energy and (iii) interfacial energy of a system composed by two crystalline phases in epitaxial relationship, are discussed. Specifically, we describe the possible 2D lattice coincidences between two phases in epitaxial relationship, as well as all of the possible initial interface configurations which generate when different surface terminations of the phases put in contact are taken into account. Then, in order to elucidate these theoretical aspects, we have studied the following epitaxies in natural systems: {110}-diamond (C)/{101}-forsterite (Mg_2SiO_4) and {001}-aragonite ($CaCO_3$)/{$\bar{1}$01}-zabuyelite (Li_2CO_3); the optimized interface structures and their adhesion energies were determined at *ab initio* level. For the diamond/forsterite system a very low value of the adhesion energy was estimated, $\beta^{D/Fo}_{(110)/(101)}$ = 0.367 J/m^2, suggesting a low probability to have epitaxy between {110}-diamond and {101}-forsterite. A higher adhesion energy was instead found for the aragonite/zabuyelite system, $\beta^{Za/Ar}_{(\bar{1}01)/(001)}$ = 0.595 J/m^2, which reveals a strong affinity between the {$\bar{1}$01}-zabuyelite and {001}-aragonite.

1. Introduction

Crystalline interfaces are the most common microstructures. They determine chemical and physical properties of devices for applications in mechanics, electronics, medicine, in material chemistry for designing and engineering of composite materials. To produce high quality materials having the desired properties was a big incentive to the research on surface and interface thermodynamics as exposed in two well-documented and exhaustive books by Sutton and Baluffi[1] and Bollman,[2] in a review on stress and strain in epitaxy[3,4] and in a paper facing the item from a historical point of view.[5] The finalization to industrial applications obscured initially the reach of the fundamental studies in fields where the interfaces cannot be neglected. It is not the scope of this paper to quote the huge number of reviews and research papers, as it is nowadays evident that an understanding of surface and interface properties is essential to deepen our knowledge in a variety of pure and applied researches. Some examples are: (i) the selection of additives as crystal habit modifiers,[6,7] (ii) the size dependent properties of associations of rock forming minerals in relation to the conditions of their formation,[8,9] (iii) the kinetics of reaction at interfaces,[10] (iv) the precipitation of minerals in natural aqueous environments as epi-layers modifying the properties of the mineral-water interface, passivating significantly the surface of the underlying minerals and determining the composition of surface water,[11,12] (v) the formation of human bones and bio-stones, (vi) the adsorption of DNA on minerals surfaces, (vii) the development of nacres platelets of oyster, and (viii) the ordered crystallization of micro and nano-phases on substrates.[13-15] There is a potential of achievements from the cross pollination between applications and natural examples. The formation of the interfaces fascinated mineralogists as Royer[16] whose systematic observations established the crystallographic and crystal chemical constraints of epitaxy. However, it was soon clear that the macroscopic bi-crystals produced in laboratories, which were in relation apparently violating Royer's deductions, form by complex mechanisms.[17,18] It became then clear the need of powerful techniques for the analysis of the interfaces, e.g. see Kern,[5] as well as theoretical and computational modeling.

This work is a contribution to the characterization of epitaxial interfaces. When, at the interface where epitaxy occurs, the misfit between 2D lattice is low, interfaces relax with negligible in plane stress and adhesion energy can be calculated without the need of considering interface dislocations. We are interested to natural systems and to the contribution that crystal growth theory can give to unravel questions such as: can olivine, $(Mg, Fe)_2SiO_4$, nucleate on some diamond faces in condition of negative affinity, or can Li be absorbed in growth sectors of some carbonate? A valid contribution to these items can only come by the coupling of the laboratory and field observations with the calculations of adhesion and interface energy. Then, in this contribution we

focus our attention on the theoretical and computational aspects related to the determinations of these thermodynamic quantities and put them in relation with real cases. Specifically, the first part of the paper concerns the individuation of the different 2D lattice coincidences between two phases in epitaxial relationship, as well as the initial structures of the interface (i.e., interface configurations) generating when the two phases are put in contact. The second part, instead, is devoted to the study of the following epitaxies: {110}-diamond (C)/{101}-forsterite (Mg_2SiO_4) and {001}-aragonite ($CaCO_3$)/{$\bar{1}$01}-zabuyelite (Li_2CO_3); the optimized interface structures and their adhesion energies were determined at quantum-mechanical level by using the B3LYP Hamiltonian[19-21] and Gaussian type basis sets. We choose these two systems for the following reasons: (i) they are interesting cases of study for elucidating the theoretical aspects discussed in the first part of this paper; (ii) a thorough knowledge of their structural and thermodynamic properties is fundamental to understand the genesis of the olivine inclusions in diamond and the ability of Li to modify the morphology of calcite/aragonite crystals growing in aqueous solution; (iii) at the best of our knowledge, this is the first time that they were studied at *ab initio* level.

2. Lattice coincidences and interface structures

2.1. How many 2D lattice coincidences?

A condition for observing epitaxy between two crystalline phases A and B, is a good 2D lattice coincidence at the A/B interface. However, it is important to stress here that this is a "necessary but not sufficient condition". Indeed, the knowledge of the adhesion energy between the phases A and B is the fundamental requirement to evaluate the probability to observe epitaxial relationships between two phases. Without this thermodynamic quantity, the only geometrical description of the 2D lattice coincidence does not allow to characterize in detail the epitaxial phenomenon. Actually, a good 2D lattice coincidence at the A/B interface is nothing else than the geometrical implication of a physical property, i.e. a good adhesion between the two epitaxial phases.

Before facing the problem of the determination of the adhesion energy, it is important to examine in depth how many 2D lattice coincidences can be found at the interface between two phases along with their differences. In order to perform this analysis, we consider two hypothetical phases (named A and B in the following) in epitaxial relationship (Fig. 1). Let's suppose that at the A/B interface it is possible to individuate the following 2D primitive (one atom per cell) rectangular lattices: (i) for the phase A (red lattice): $a_1 = 16$, $b_1 = 8$, $\gamma = 90°$; (ii) for the phase B (blue lattice): $a_1 = 20$, $b_1 = 10$, $\gamma = 90°$. In this case the parametric misfits result to be $\delta_{a1} = 4$ (25%) and $\delta_{b1} = 2$ (25%). We have labeled this epitaxial coincidence with the number 1 (region 1, blue area in Fig. 1).

Now, it is interesting to analyze the variation of the parametric misfits when these 2D lattices are increased in size, that is when 2D supercells are considered. The following cases can arise:

(i) A (2×2)-supercell for both phases is taken into account (region 2, pink area in Fig. 1). Then, for the phase A the parameters are: a_2 = 32, b_2 = 16; for the phase B: a_2 = 40, b_2 = 20; the misfits are δ_{a2} = 8 (25%) and δ_{b2} = 4 (25%). We have the same parametric misfit (25%) observed for the region 1, as well as an equal number of atoms (i.e., 4 atoms in both (2×2)-supercells).

(ii) (3×3)- and (2×2)-supercells for phases A and B, respectively, are considered (region 2, pink area in Fig. 1). In this case, the cell parameters for phase A are a_2 = 48 and b_2 = 24, whereas for the phase B they are a_2 = 40 and b_2 = 20, the same of case (i). Interestingly, the same percentage variation is observed for the 2D cell parameters, being δ_{a2} = 8 (25%) and δ_{b2} = 4 (25%). But, with respect to case (i), the number of atoms involved is different: the (3×3)-supercell of A has 9 atoms, whereas the (2×2)-supercell of B has only 4 atoms.

(iii) (4×4)- and (3×3)-supercells for phases A and B, respectively, are considered (region 3, yellow area in Fig. 1). The cell parameters of A are a_3 = 64 and b_3 = 32, while those of B are a_3 = 60 and b_3 = 30. With respect to the cases (i) and (ii), the parametric misfit is reduced, having δ_{a3} = 4 (~ 7%) and δ_{b3} = 2 (~ 7%), whereas the discrepancy between the number of atoms in the two supercells is increased, with 16 atoms in the (4×4)-supercell of A and 9 atoms in the (3×3)-supercell of B.

(iv) (5×5)- and (4×4)-supercells for phases A and B, respectively, are considered (region 4, Fig. 1). In this case, a perfect parametric coincidence ($\delta_{a4} = \delta_{b4} = 0$) between the two 2D lattices is observed, with a_4 = 80 and b_4 = 40; this is the case of a free strain system. The discrepancy between the number of atoms in the two supercells is further increased, with 25 atoms in the (5×5)-supercell of A and 16 atoms in the (4×4)-supercell of B.

For the sake of simplicity, we have only discussed the epitaxies describable with (n×n)-supercells, but it is licit also to use (m×n)-supercells, where m ≠ n. As an example, (1×4)- and (1×3)-supercells for phases A and B, respectively, can be considered. For such a case, the cell parameters of the phase A are a_1 = 16 and b_4 = 32, and those of the phase B are a_1 = 20 and b_3 = 30. The parametric misfits result to be δ_{a1} = 4 (25%) and δ_{b3} = 2 (~ 7%), and the number of atoms in the (1×4)- and (1×3)-supercells is 4 and 3, respectively.

According to the terminology universally accepted concerning epitaxy, when the lattice constants of phases A and B match, that is when (1×1)-A ≡ (1×1)-B, the interface is said *coherent*; when a relation such as (m×n)-A ≡ (k×s)-B exists, with m, n, k and s integers (and the lengths

supercells parameters are not too long on the lattice length scale), the interface is *commensurate*; otherwise it is *incommensurate*.

We have only discussed rectangular (or squared) 2D meshes, but oblique 2D lattices should be also taken into account. At variance with the rectangular case, it is more unlikely to have epitaxial coincidences describable with large oblique supercells. This is evident by observing Fig. 1b, where in addition to the lattice parameters a and b, the angle θ must be also considered for describing the lattice coincidence. Indeed, also with a small angular mismatch, to have a good coincidence between the areas of the 2D lattices (red and blue in Fig. 1b) can be difficult, due to the divergence of the lattices parameters when increasing the size of the supercells.

The purpose of the example just discussed is to draw attention to the different cases that can arise when studying epitaxial phenomena. For real systems, where the 2D cell parameters are never natural numbers, the observable cases are more complex and less distinct, but always ascribable to the ones previously described. As an example of real case, we consider the epitaxy identified between α-quartz (SiO_2; S.G. $P3_12$) and witherite ($BaCO_3$; S.G. *Pmcn*).[22] Bittarello et al.[22] observed heterogeneous nucleation of {001}-witherite lamellae onto three different forms of α-quartz: the prism {10.0} along with the rhombohedra {10.2} and {01.2}; the witherite lamellae are epitaxially oriented along the [100], [001] and $[21\bar{1}]$ of α-quartz. By taking into accounts the 3D cell parameters used by Bittarello et al.,[22] it is possible to identify the 2D lattice coincidences reported in Table 1 for the {10.0}-quartz/{001}-witherite epitaxy. The same epitaxial relationship can be described by means of two different combinations of supercells having the same orientation: the first one (n. 1, Table 1) is given by the (1×2)- and (1×1)-supercells for α-quartz and witherite, respectively; the second one (n. 2, Table 1), instead, by the (7×2)- and (6×1)-supercells. In both cases the parametric misfit is low (Table 1), but a different amount of matter is included in the supercells. As a matter of fact, by supposing one atom per (1×1)-cell for both the phases involved, for the case n.1 we have an atomic ratio of 2/1 (i.e., since there are 2 atoms in the (1x2)-cell of α-quartz and 1 atom in the (1×1)-cell of witherite), whereas for the case n. 2, the atomic ratio is greater (14/6 = 2.3). The only way to individuate the most probable epitaxial coincidence (i.e., the structure of the interface) is to calculate the adhesion energy (or the corresponding interfacial energy) between the two phases for each 2D lattice: lower the adhesion energy, lower the probability to observe that reticular mesh. Unfortunately, a large 2D lattice requires to manage a system made by hundreds or thousands of atoms, then in the majority of the cases the simulation approach is not feasible due to a prohibitive computational effort.

An interesting computational work concerning the use of supercells with increasing size for determining the adhesion energy, was performed by Irving et al.[23] They studied the (111)-Ag/(110)-

GaAs interface (i.e., a monolayer of Ag in epitaxy on a GaAs substrate) by performing DFT calculations and determining that the adhesion energy calculated for different sizes of supercells can be very similar in some cases and very different in other ones. Furthermore, they observed that the choice of the computational unit cell has effects on both the atomic structure and the calculated adhesion energy, since a strain is generated into the metallic layer (i.e., monolayer of Ag) in the Ag(111)/GaAs(110) system. The extent of the effects is dependent not only on the magnitude but also on the type of the induced strain (i.e, tensile and compressive strain into the monolayer of Ag). Therefore, this work outlines once more the importance of analyzing different computational unit cells when studying epitaxial phenomena.

Table 1. Some epitaxial lattice coincidences between witherite and α-quartz when witherite lamellae are perpendicular to the {10.0} faces and to the [001] axis of α-quartz.

n.	Vectors of the 2D cell of α-quartz(Å)	Vectors of the 2D cell of whiterite(Å)	misfit (%)
1	<100> = 4.9134	[100] = 5.3126	8.1
	2×<100> = 9.8320	[110] = 10.3614	5.4
2	7×<100> = 34.3938	6×[100] = 31.8756	-7.9
	2×<100> = 9.8320	[110] = 10.3614	5.4

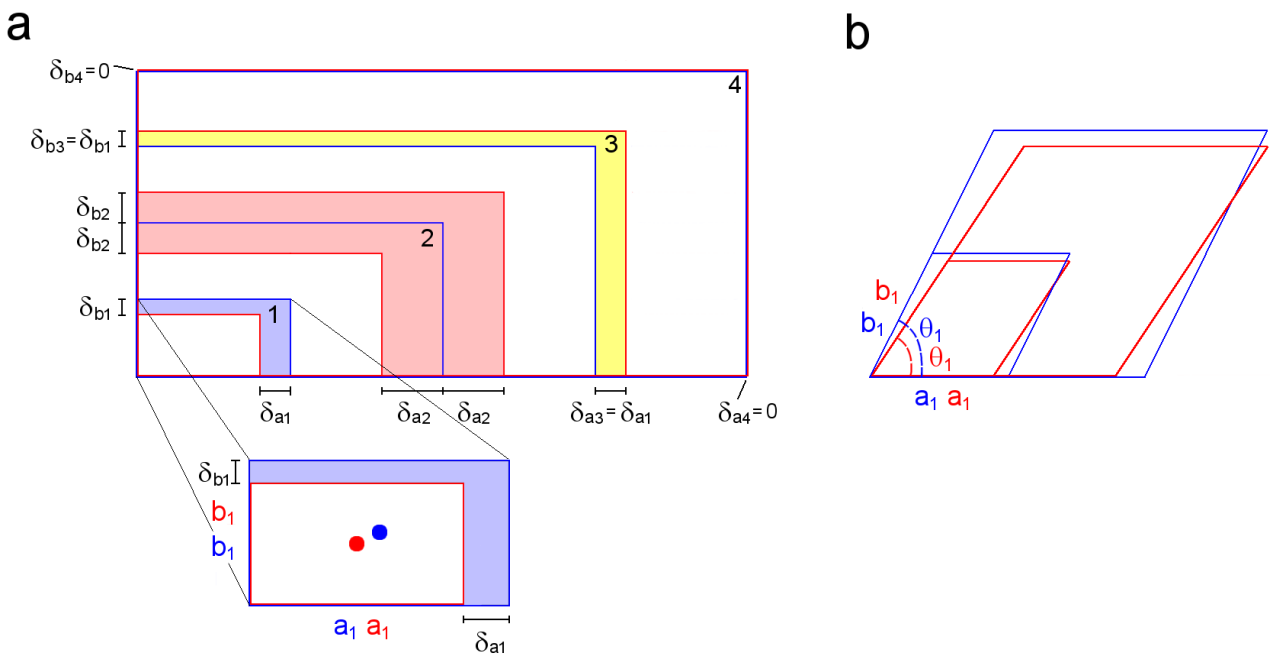

Figure 1. A schematic drawing of some 2D lattice coincidences that can be found for a generic A/B interface.

2.2. How many interface structures?

There is a further argument to discuss when the epitaxy occurs between chemically and structurally complex phases. The crystal faces, $(hkl)^A$ and $(h'k'l')^B$ (Fig. 2a), that are put in contact for generating the composed slab A/B/A, can show a huge number of initial surface configurations (or surface terminations); with the term *initial*, we mean the surface termination obtained by cutting the bulk structure without performing the optimization of the surface structure. As we demonstrated in two recent papers,[24,25] finding these configurations is a very difficult task that requires a careful analysis of both structure and symmetry of the surface. In these papers all of the possible initial surface configurations of some crystal faces of pyrope ($Mg_3Al_2Si_3O_{12}$) and $MgAl_2O_4$ spinel were determined: as an example, 48 and 52 different surface terminations were identified for the (100) face of pyrope and $MgAl_2O_4$ spinel, respectively.

As concerns the interface, this means that when a composed slab is formed by two crystal faces $(hkl)^A$ and $(h'k'l')^B$ showing *m* and *n* surface terminations, respectively, the number of possible initial interface configurations to take into accounts is $m \times n$. In practice, this makes difficult, or impossible in some cases, the determination of the "most stable" interface structure, namely that showing the highest adhesion energy. Indeed, in some cases the number of structural optimizations to perform could become extremely high and hence, not practicable.

A possible strategy to reduce drastically the number of initial interface configurations to analyze, is here proposed and is based on our findings on the stability of the crystal surfaces. Recently, different crystal faces of calcite ($CaCO_3$), halite (NaCl), gypsum ($CaSO_4 \cdot 2H_2O$) and hydroxyapatite ($Ca_5(PO_4)_3(OH)$) were studied in our research group by means of quantum-mechanical and empirical calculations. The surface energy of all of them were calculated at 0K, by considering different surface terminations in contact with the vacuum. For each face, it was observed that among all the considered surface terminations the most stable one resulted to be that respecting the bulk symmetry of the crystal. Then, as stated in the paper by Bruno:[26] "… *the bulk crystal symmetry has to be necessarily considered to achieve the self-consistency of the surface termination: the symmetry group of a surface termination must be a subgroup of the symmetry of the bulk crystal viewed along the normal to the surface*". The same concept was also expressed by means of the Curie's symmetry principle[27] as follows: "*the symmetry group of a crystal face in its mother phase is given by the maximal common subgroup of the symmetry group of the bulk crystal and of the symmetry group of the mother phase*. *For the crystal/vacuum system, only the symmetry group of the crystal bulk can impose constraints on the symmetry group of the face. Then, according to the Curie's principle the face should have the maximal subgroup of the symmetry of the crystal bulk projected along the normal to the surface*".

We can extend these results to the case of the interface between two crystalline phases A and B, that is: the symmetry group of a crystal interface is given by the maximal common subgroup of the symmetry groups of the slabs A and B. Otherwise stated, the most probable interface configuration should be that preserving the highest number of symmetry elements in common between the two slabs A and B.

3. Computational details

To investigate the interface structure between two phases in epitaxial relationship, a 2D periodic slab model[28] and the *ab initio* CRYSTAL09 code[29-31] were adopted. The calculations were performed by using the B3LYP Hamiltonian,[19-21] which provided accurate results for the surface properties of the minerals considered in the present work.[32] Further computational details (e.g., basis set, thresholds controlling the accuracy of the calculations) are reported in the Supporting Information.

A composed slab (A/B/A; Fig. 2a), made by the phases A and B (slab A and B in the following), was generated in the following way: (i) the slabs A and B of a given thickness were made by cutting their respective bulk structures parallel to the *hkl* planes of interest and using the same 2D cell parameters describing the epitaxy; (ii) the slab B was placed in between two slabs A; (iii) then, the composed slab geometry (atomic coordinates and 2D cell parameters) was optimized by considering all the atoms free to move. The composed slab A/B/A was generated preserving the center of inversion or a mirror plane parallel to the face, and ensuring the vanishing of the dipole moment perpendicular to the slab. The CRYSTAL09 output files, listing the optimized fractional coordinates and optimized 2D cell parameters of the composed slabs, are freely available at http://mabruno.weebly.com/download).

The calculations were done by considering composed slabs with a thickness sufficient to obtain an accurate description of the interfaces. The slab thickness is considered appropriate when the bulk-like properties are reproduced at the centre of the slabs A and B.

The specific adhesion energy, $\beta^{A/B}_{(hkl)/(h'k'l')}$ (J/m^2), is the "*energy gained*" once the boundary interface is formed; it reads:

$$\beta^{A/B}_{(hkl)/(h'k'l')} = \frac{E(2A) + E(B) - E(2A+B)}{S} \quad (1)$$

where $E(2A+B)$, $E(2A)$ and $E(B)$ are the static energies (at 0K) of the optimized slab A/B/A (Fig. 2a), slab A/vacuum/A (Fig. 2b) and slab B (Fig. 2c), respectively, and S is the area of the surface unit cell.

The specific interfacial energy, $\gamma^{A/B}_{(hkl)/(h'k'l')}$ (J/m^2), is the "*excess energy*" resulting from the energy balance described by the Dupré's relation:

$$\gamma^{A/B}_{(hkl)/(h'k'l')} = \gamma^{A}_{(hkl)} + \gamma^{B}_{(h'k'l')} - \beta^{A/B}_{(hkl)/(h'k'l')} \quad (2)$$

where $\gamma^{A}_{(hkl)}$ and $\gamma^{B}_{(h'k'l')}$ are the specific surface energies of the (*hkl*) and (*h'k'l'*) faces delimiting the slabs A and B, respectively. These "*energies to be spent*" are calculated through the well-known equation:

$$\gamma^{i}_{(hkl)} = \frac{E(i) - E_b(i)}{2S}\,;\ i = \text{A, B} \quad (3)$$

where $E_b(i)$ is the energy of the bulk of the *i*-th phase and the factor of 2 in the denominator accounts for the upper and lower surfaces of the slab model.

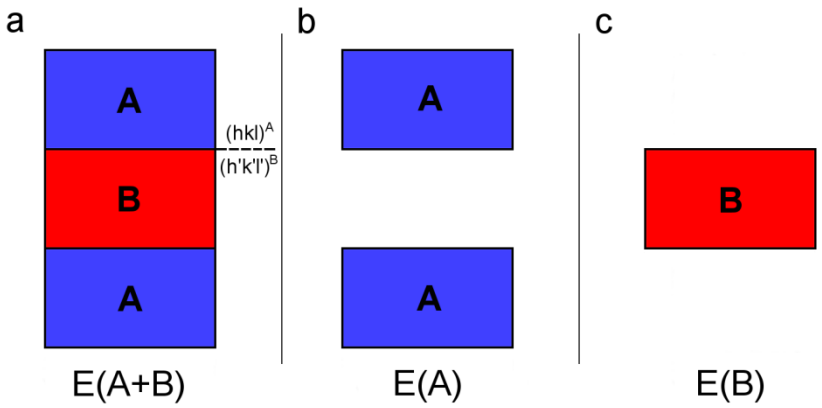

Figure 2. Schema for building and performing the calculation on a composed slab A/B/A.

4. Diamond/forsterite epitaxy

4.1. Why to study this epitaxy

The determination of the crystallographic orientation of the olivines (i.e., a solid solution between the two end members forsterite, Mg_2SiO_4, and fayalite, Fe_2SiO_4; S.G. *Pbnm*) included in diamond is

of paramount importance in diamond studies. It was suggested that an epitaxial relationship between the inclusion and its host would represent a robust proof of syngenesis;[33-36] we use the term "syngenesis" in its restrictive meaning given by Nestola et al.:[37] the syngenesis is the simultaneous growth of the inclusion and host, which can co-precipitate from the same medium.
In a recent work[37] the crystallographic orientations of 47 olivines incorporated in 21 diamonds from Udachnaya kimberlite (Siberia) were analyzed, and at variance with the previous findings of Mitchell and Giardini,[38] no preferential orientation was observed between olivine and diamond. On this basis, a protogenetic origin was hypothesized for these olivines: that is, pre-existing olivines ware passively incorporated into growing diamonds.

A fundamental contribution to the debate about syngenesis or protogenesis can be obtained by the determination of the adhesion energy between olivine and diamond. The theoretical epitaxial relationships between these two phases are numerous, but the most interesting among them are reported in Table 2, where the 2D lattice coincidences are also listed. From a computational point of view, we were not able to perform the calculations only for the {111}-diamond/{010}-olivine epitaxy. The study of this epitaxy requires the construction of a slab composed by a huge number of atoms (i.e., a large 2D cell of 340 $Å^2$) whose geometry optimization is not workable with the resources of calculus actually at our disposition (i.e., a cluster with 400 CPU).

In this paper we only report and discuss the epitaxy between {110}-diamond and {101}-forsterite. The other interfaces will be the subject of a future publication in which a detailed comparison between their structures and adhesion energies will be done. Moreover, since the most common olivines in diamond are richer in magnesium than in iron (i.e., forsterite ~ 92%) and to further simplify the system-model, we performed the calculations by only considering a pure forsterite. A positive peculiarity of this interface is the existence of only one possible configuration, which is due to the fact that both (110) face of diamond and (101) of forsterite display a unique surface termination.[32,39]

It is important to remember that, at variance with the (100) and (111) faces, the (110) one of diamond does not undergo any reconstruction. Indeed, a simple relaxation of the first two atomic layers is sufficient to create a π-bonded 'zig-zag' chain over the surface, with distances and angles very close to the values of the reconstructed (111)-2×1(Pandey reconstruction) diamond surface (see De La Pierre et al.[39] for further details and references). Then, the simple relaxed configuration of the (110) face saturates the fourth dangling bond of surface carbons, with a stabilization effect. For this reason we have only considered in this work an unreconstructed (110) face; a reconstructed (110) face was never observed. Furthermore, De La Pierre et al.[39] have studied at *ab initio* level the reconstructed and unreconstructed (100) and (111) faces, and the unreconstructed (110) face of

diamond: the structures and surface energies were determined and compared with previous *ab initio* calculations carried out with different methodologies. Then, they have shown that the structural properties and surface energies for the three crystal faces, obtained with the same basis sets and functional of the present work, are in good agreement with previous pure DFT studies. For this reason we believe that the basis sets and functional (B3LYP) adopted to study the (110)-diamond/(101)-forsterite interface are able to describe in a reliable way the electronic distribution, the structural properties and the energy of the system.

In order to verify the criterion of convergence on the thickness of the slabs A (diamond) and B (forsterite), four composed slabs were considered (Table 3): (i) a composed slab formed by a slice of forsterite (Fo) with thickness equal to $2\times d_{101}$ (d_{hkl} being the spacing between two successive *hkl* planes) placed between two slices of diamond (D) having a thickness of $1\times d_{110}$ (shortened in the following as 1D/2Fo/1D); (ii) 2D/2Fo/2D; (iii) 3D/2Fo/3D; (iv) 1D/3Fo/1D.

Table 2. 2D lattice coincidences between diamond and forsterite, and aragonite and zabuyelite. The bulk lattice constants of diamond, forsterite, aragonite and zabuyelite are taken from Hom et al.,[40] Merli et al.,[41] de Villiers,[42] and Effenberger and Zemann.[43] We also report |Δ(%)| = |(area forsterite – area diamond)/area forsterite)|×100, to stress the area variation between the 2D cells.

	faces	a (Å)	b (Å)	a^b (°)	area (Å^2)	|Δ(%)|
diamond	{001}	[110]=5.05	2×[1$\bar{1}$0]=10.10	90	51.01	4.9
forsterite	{001}	[100]=4.76	[010]=10.22	90	48.65	
diamond	{001}	[110]=5.05	2×[1$\bar{1}$0]=10.10	90	51.01	16.7
forsterite	{100}	[001]=5.99	[0$\bar{1}$0]=10.22	90	61.22	
diamond	{110}	2×[10$\bar{1}$]=10.10	2×[010]=7.14	90	72.11	7.8
forsterite	{101}	[010]=10.22	[$\bar{1}$01]=7.65	90	78.18	
diamond	{111}	[$\bar{1}$01]=5.05	2×[0$\bar{1}$1]=10.10	60	44.17	9.2
forsterite	{001}	[100]=4.76	[110]=11.27	65	48.62	
diamond	{111}	3×[$\bar{1}$01]=15.15	5×[0$\bar{1}$1]=25.24	60	331.16	3.1
forsterite	{010}	2×[101]=15.30	2×[$\bar{1}$02]=25.78	60	341.60	
aragonite	{001}	[100]=4.96	[010]=7.97	90	39.53	4.9
zabuyelite	{001}	[010]=4.97	[100]=8.36	90	41.55	
aragonite	{001}	[100]=4.96	[010]=7.97	90	39.53	1.2
zabuyelite	{$\bar{1}$01}	[010]=4.97	[101]=8.05	90	40.01	

Table 3. Optimized 2D cell parameters, adhesion and interfacial energies for the {110}-diamond/{101}-forsterite and {001}-aragonite/{$\bar{1}$01}-zabuyelite epitaxies. The interfacial energies are calculated through eq. (2) and the following surface energy values: $\gamma^{D}_{(110)}$ = 5.046, $\gamma^{Fo}_{(101)}$ = 1.696, $\gamma^{Ar}_{(001)}$ = 0.612 and $\gamma^{Za}_{(\bar{1}01)}$ = 0.280 J/m^2.

slab	atoms	a (Å)	b (Å)	a^b (°)	area (Å^2)	$\beta^{A/B}_{(hkl)/(h'k'l')}$ (J/m2)	$\gamma^{A/B}_{(hkl)/(h'k'l')}$ (J/m^2)
{110}-diamond/{101}-forsterite							
1D/2Fo/1D	152	7.8436	10.0253	90.00	78.63	0.974	5.768
2D/2Fo/2D	216	7.5510	10.0144	90.06	75.62	0.378	6.364
3D/2Fo/3D	280	7.4210	10.0444	90.09	74.54	0.367	6.375
1D/3Fo/1D	180	7.8634	10.1196	90.11	79.57	1.070	5.672
{001}-aragonite/{$\bar{1}$01}-zabuyelite							
6Za/6Ar/6Za	204	4.9635	8.1060	90.11	40.23	0.595	0.297

4.2. Structure and energy of the {110}-diamond/{101}-forsterite interface

The optimized cell parameters of the different composed slabs are listed in Table 3, whereas the relaxed structure of the 3D/2Fo/3D slab is reported in Fig. 3. A detailed structural analysis of the interface is out of the scope of this work, therefore only a qualitative and short description is given in the following. People interested to an in-depth structural analysis can carry out it by using the CRYSTAL09 output file reporting the optimized atomic coordinates.

A strong structural modification at the diamond/forsterite interface is observed (Fig. 3). The (110) surface of diamond is a very compact one and undergoes a slight structural relaxation when in contact with the vacuum.[39] But when this surface is put in contact with the forsterite (101), an evident geometry modification exhibits with a strong *roughness* of the C layer adjacent to forsterite. In order to give an idea, for the C layer in contact with vacuum Δz (i.e., the difference between the z coordinates of the C atoms in the same layer) is 0.0038 Å, whereas for the layer in contact with forsterite Δz reaches 0.1966 Å. In a similar way, the (101) slab of forsterite is considerably affected by the presence of the diamond. A clear evidence of this phenomenon is the strong distortion of the SiO_4 tetrahedra in proximity of the diamond (Fig. 3a). As a consequence of this structural arrangement at the interface, the formation of two C-O bonds, whose lengths are 1.3960 and 1.4330 Å, is observed.

It is worth noting that, despite all of these structural modifications, the extreme rigidity of the (110) surface of diamond and the noteworthy difference of chemical composition between the two phases, do not allow to obtain a {110}-diamond/{101}-forsterite interface with a compact structure. Instead, a very *open* interface structure is generated, as it results particularly evident by

observing Fig. 3b. Such structural incompatibility between these two phases generates a very low adhesion energy, $\beta^{D/Fo}_{(110)/(101)}$ = 0.367 J/m^2 (Table 3) and, accordingly, a very high interfacial energy, $\gamma^{D/Fo}_{(110)/(101)}$ = 6.375 J/m^2. It is interesting to observe that $\beta^{D/Fo}_{(110)/(101)}$ corresponds to ~5% of the highest possible value of adhesion energy for this interface, that is 6.742 J/m^2, which is obtained by considering $\gamma^{D/Fo}_{(110)/(101)}$ = 0 in eq. (2).

To test the reliability of such values, we verified the convergence criterion by performing the calculations on systems with different thickness; in particular, the adhesion energy for these systems was calculated. By analyzing the data listed in Table 3, one observes that the adhesion energy rapidly converges to a value of the order of ~0.370 J/m^2, when the thickness of the diamond slab is increased and that of forsterite is kept fixed. Then, a diamond slab having a thickness of $2\times d_{110}$ (2D) seems to be sufficient for verifying the criterion of convergence.

Later on, we carried out the calculations on a 1D/3Fo/1D composed slab. The corresponding value of the adhesion energy is 1.070 J/m^2, which is only ~10% higher than that obtained for the 1D/2Fo/1D slab. Therefore, at this level of numerical precision, obtained by using not particularly rich all-Gaussian basis sets, that can be considered a good compromise between accuracy and computing costs, we believe that our estimate of adhesion energy is reliable. Indeed, richer basis sets could modify our values of the same order of magnitude observed for the 1D/3Fo/1D composed slab.

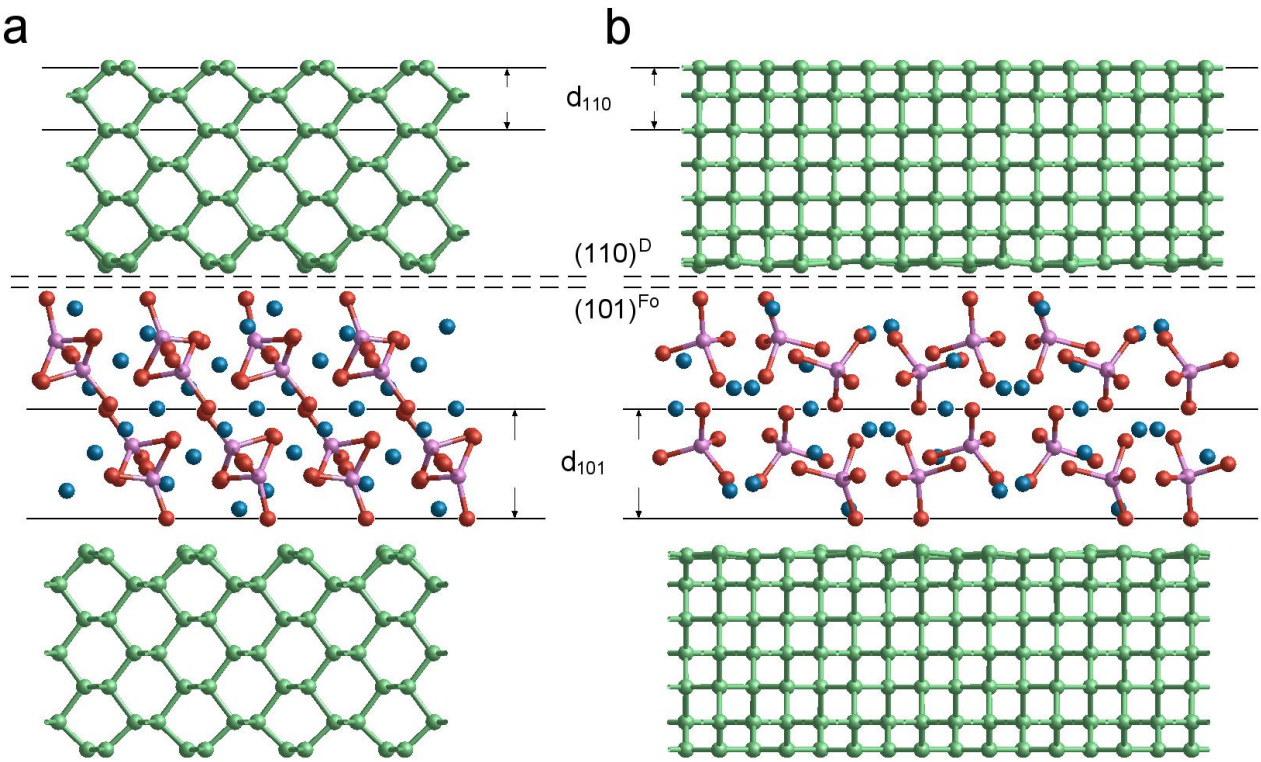

Figure 3. {110}-diamond/{101}-forsterite interface viewed along the <010> (a) and $<\bar{1}01>$ (b) directions of forsterite. Spacing d_{110} of diamond and d_{101} of forsterite are also shown. Mg, Si, O and C are blue, pink, red and green, respectively.

Unfortunately, we are not able to compare our estimate of adhesion energy with previous ones, since this is the first time, at the best of our knowledge, that similar calculations have been performed on diamond/forsterite system. On the other hand, it is interesting to briefly discuss the meaning of such a high value of the interfacial energy (6.375 J/m^2), in particular when compared to the surface energy values of the (110) and (101) faces of diamond (5.046 J/m^2) and forsterite (1.696 J/m^2), respectively. According to the classical nucleation theory, all the more the adhesion energy is high, all the more the heterogeneous nucleation of a 3D phase (i.e., the formation of 3D nuclei of a phase A above a phase B) is favored with respect to the homogeneous one. In the specific case, we obtained a very low adhesion energy, suggesting a very low probability to observe epitaxy between {110}-diamond and {101}-forsterite. This is in agreement with the experimental observations that never reported such an epitaxy. However, further energy calculations on other types of diamond/forsterite epitaxy (see Table 2) must be performed for discussing in more detail the reciprocal orientations between diamond and the included olivine.

5. Aragonite/zabuyelite epitaxy

5.1. Why to study this epitaxy

Aragonite (S.G. *Pmcn*) is one of the two commonly occurring polymorphs of calcium carbonate ($CaCO_3$) (the other one is calcite) found in geological and biological systems, whereas zabuyelite is a very uncommon monoclinic carbonate (Li_2CO_3; S.G. *C2/c*) discovered in the Zabuye Salt Lake (Tibet), where it occurs as small crystals (1.5–20 μm) embedded in halite (NaCl; see Anderson et al.,[44] and references therein).

The influence of Li on the growth morphology of calcium carbonate crystals (calcite) is well known and was discussed for the first time by Rajam and Mann[45] and Nefyodova[46] who found the appearance of the {0001} pinacoid in addition to the cleavage rhombohedron in calcite crystals growing from aqueous solution in the presence of Li. The stabilization of the kinked {0001} form was explained in terms of random adsorption of Li that slows down the growth rate of the surface. Recent studies on calcite growth from aqueous solutions in the presence of variable concentrations of Li and on the growth morphology of Li_2CO_3 crystals (zabuyelite)[47-49] proved that, in the presence of Li, the character of the {0001} and $\{01\bar{1}8\}$ forms of calcite changes respectively from kinked

and stepped to flat. This behavior was explained in terms of epitaxial agreement between calcite and zabuyelite. Actually, the presence of very high concentrations of Li into the solution (approximately Li/Ca molar ratio higher than 14, ionic strength higher than 3, and very high supersaturation with respect to calcite) determines both the modification of the character of some forms of calcite as previously stated, and the growth of a secondary calcium carbonate phase (aragonite). Aragonite crystals obtained under these conditions show a pseudo-hexagonal morphology due to the repeated twinning on the 110 plane.

A transition between calcite with modified morphology and aragonite occurs, depending on the Li/Ca ratio in solution: as the concentration of Li in the solution increases, the morphology of calcite turns from the cleavage rhombohedron to a flat pseudo-hexagonal shape dominated by the pinacoid. When the cation ratio exceeds the critical value of 14, a new phase (aragonite) forms. Details about the experimental and theoretical study of the relationships between aragonite and zabuyelite will be discussed in a forthcoming paper.

Two interesting epitaxies can be found for the zabuyelite/aragonite system (Table 2), having both a small surface area of the common 2D mesh. In the following we only discuss the epitaxy between {001}-aragonite and $\{\bar{1}01\}$-zabuyelite. The other one will be reported in a forthcoming paper, in which the experimental observations will be coupled with a detailed computational study of all the interface structures and adhesion energies. Two possible initial configurations can be recognized for the {001}-aragonite/$\{\bar{1}01\}$-zabuyelite interface, since the (001) face of aragonite display two surface profiles (i.e., Ca and CO_3 terminated). This is the consequence of the bulk structure of aragonite, which consists of alternating layers of Ca and CO_3 ions stacked along the [001] axis; for a more detailed discussion of the main faces of the aragonite see the papers by Massaro et al.[50] and Aquilano et al.[51] For the sake of simplicity we only analyzed the interface formed by the CO_3 terminated (001) face of aragonite, as well as only a composed slab (Table 3) formed by a slice of aragonite (Ar) with thickness equal to $6\times d_{001}$ placed between two slices of zabuyelite (Za) having a thickness of $6\times d_{\bar{1}01}$ (6Za/6Ar/6Za), was considered.

5.2. Structure and energy of the {001}-aragonite/$\{\bar{1}01\}$-zabuyelite interface

The optimized cell parameters of the slab are listed in Table 3, whereas the relaxed structure is reported in Fig. 4. As for the diamond/forsterite system, a detailed structural analysis can be performed by downloading the CRYSTAL09 output file.

At variance with the diamond/forsterite case, a minor structural modification of the interface is observed (Fig. 4), with only the two layers in contact that result to be affected by a visible

geometry relaxation. In particular, the CO_3 groups of the zabuyelite adjacent to the aragonite are considerably tilted with respect to their position in the bulk (i.e., at the center of the slab of zabuyelite) and in the layer exposed to the vacuum. Instead, a more rigid behavior of the aragonite layer next to zabuyelite is observed: the CO_3 groups are only slightly tilted with respect to the bulk. Then, it is evident that the zabuyelite is able to adjust its own ($\bar{1}01$) surface structure to generate a good structural continuity with the (001) face of aragonite. This structural compatibility is also highlighted by a high value of the adhesion energy, $\beta^{Za/Ar}_{(\bar{1}01)/(001)}$ = 0.595 J/m^2 (Table 3). It follows a low interfacial energy value, $\gamma^{Za/Ar}_{(\bar{1}01)/(001)}$ = 0.297 J/m^2, which is almost equal to that of the surface energy of the ($\bar{1}01$) face of zabuyelite ($\gamma^{Za}_{(\bar{1}01)}$ = 0.280 J/m^2). The adhesion energy $\beta^{Za/Ar}_{(\bar{1}01)/(001)}$ corresponds to 67% of its highest possible value for this interface (0.892 J/m^2), unveiling a very different behavior with respect to the one of the diamond/forsterite interface. But as for the latter, there are not previous computational estimates of such thermodynamic quantities related to the {001}-aragonite/{$\bar{1}01$}-zabuyelite interface.

A so high adhesion energy suggests a strong predisposition of the {$\bar{1}01$}-zabuyelite to arrange above the{001}-aragonite or vice versa. An adsorption is to be expected eventually followed by an absorption of Li_2CO_3 during the growth of aragonite in aqueous solution in the presence of Li, in analogy with the experimental finding by Pastero et al.[47] and Pastero and Aquilano[49] where a 2D epitaxial growth mechanism between calcite and zabuyelite was described.

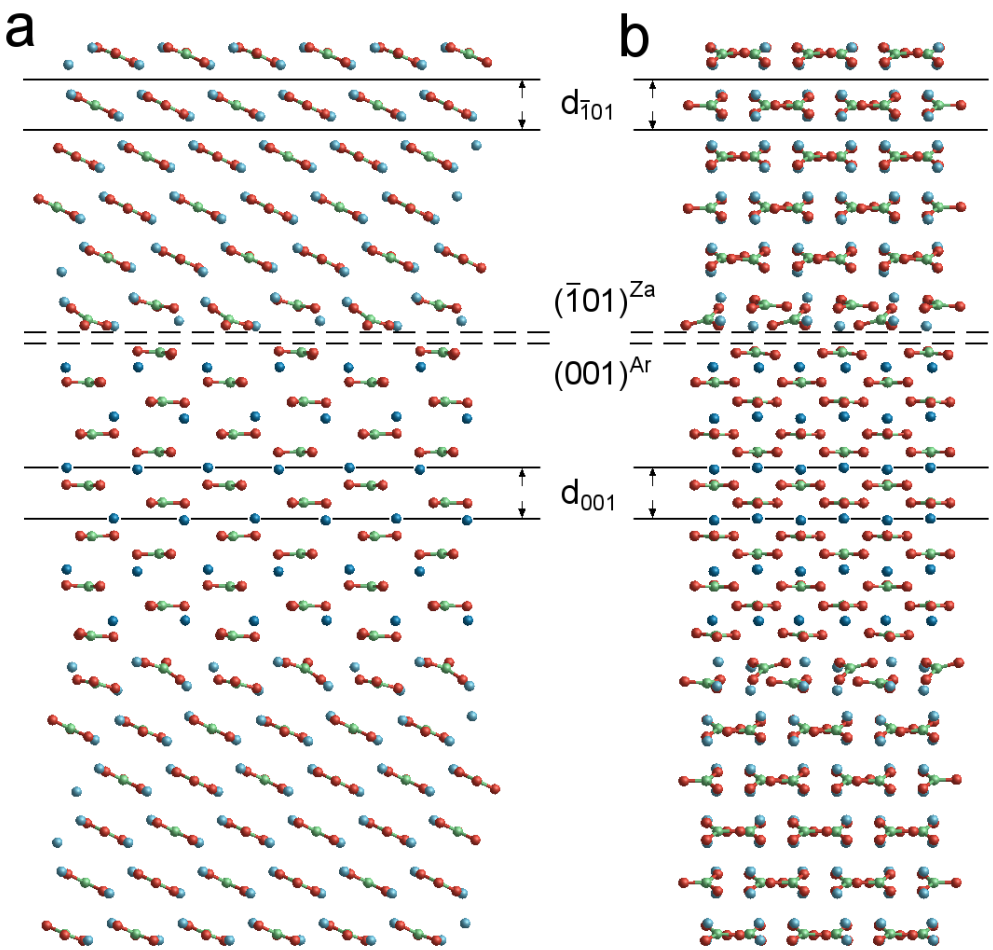

Figure 4. {001}-aragonite/{$\bar{1}$01}-zabuyelite interface viewed along the <100> (a) and <010> (b) directions of aragonite. The d_{001} spacing of aragonite and $d_{\bar{1}01}$ of zabuyelite are also shown. Ca, Li, O and C are blue, pale blue, red and green, respectively.

6. Conclusions

This work is subdivided in two parts: (i) the first one, in which we describe how to determine all of the possible 2D lattice coincidences between two phases in epitaxial relationship, as well as the initial interface structures which are generated by considering different surface terminations; (ii) the second one, where the structure and energetic of the {110}-diamond/{101}-forsterite and {001}-aragonite/{$\bar{1}$01}-zabuyelite interfaces are determined by means of *ab initio* quantum-mechanical simulations. In particular, in this paper we have highlighted the difficulties encountered when the study of the epitaxy is faced at computational level, difficulties that are mainly due to the occurrence of the numerous 2D lattice coincidences and surface terminations of the phases involved in the epitaxy.

We can summarize our results as follow:

(i) The epitaxy between two phases can be described by means of 2D supercells having very different surface areas and, as a consequence, different atomic density at the interface. The only way to establish the most probable 2D lattice of coincidence is to calculate the adhesion energy for all of the possible cases: higher the adhesion energy value, higher the probability to observe the corresponding 2D coincidence lattice.

(ii) When studying chemically and structurally complex phases in epitaxial relationship, the number of the initial interface structures to consider can be enormous. From a computational point of view, this could make difficult the determination of the most stable interface structure (i.e. the interface with the highest adhesion energy). By extending our previous studies on the symmetry of the crystal surfaces, we suggest that the most probable interface configuration should be that preserving the highest number of symmetry elements in common between the two slabs forming the composed one. If this work hypothesis is correct, the number of initial interface configurations to evaluate should decrease significantly.

(iii) The structure of the {110}-diamond/{101}-forsterite and {001}-aragonite/{$\bar{1}$01}-zabuyelite interfaces was determined by means of *ab initio* calculations. The adhesion and interfacial energies for the two systems were also evaluated. For the diamond/forsterite system a very low value of the adhesion energy was estimated, $\beta^{D/Fo}_{(110)/(101)}$ = 0.367 J/m^2, suggesting a low probability to have epitaxy between {110}-diamond and {101}-forsterite. A higher adhesion energy was found instead for the aragonite/zabuyelite system, $\beta^{Za/Ar}_{(\bar{1}01)/(001)}$ = 0.595 J/m^2, which reveals a strong affinity between the {$\bar{1}$01}-zabuyelite and {001}-aragonite.

(iv) We do not claim that the values of the adhesion and interfacial energies reported in this paper could be definitive. When dealing with these thermodynamic quantities at quantum-mechanical level, a rigorous work of assessment of the accuracy of the calculations must be performed. In particular, various Gaussian-type basis sets and several formulations for the exchange-correlation functional within the Density Functional Theory (DFT) should be evaluated, but the size of the systems studied in the present work prevents such a detailed analysis. Nevertheless, the order of magnitude of the values we obtained are very useful to interpret the experimental observations.

Acknowledgements

The work was supported by the European Research Council Starting Grant 2012 under grant agreement 307322 to F. Nestola (project INDIMEDEA; www.indimedea.eu). Thanks are due to two

anonymous reviewers for their careful reading of the manuscript and their fundamental observations on our work.

Supporting Information Available. Computational details for the *ab initio* simulations. This material is available free of charge via the Internet at http://pubs.acs.org.

References

(1) Sutton, A.P.; Balluffi, R.W. *Interfaces in Crystalline Materials*; Clarendon Press: Oxford,1996.
(2) Bollman, W. *Crystal defects and crystalline interfaces*; Springer: Berlin, 1970.
(3) *Stress and Strain in Epitaxy: theoretical concepts, measurements and Applications*; Hannbücken, M.; Deville, J. Eds.; Elsevier, 2001.
(4) Müller, P.; Saúl, A. *Surface Sci. Rep.* **2004**, *54*, 157-258.
(5) Kern, R. *Cryst. Res. Technol.* **2013,** *48*, 727-782.
(6) *Advances in crystal growth inhibition technologies*; Amjad, Z., Ed.; Plenum Press: New York, 2000.
(7) *Mineral scale formation and inhibition*; Amjad, Z., Ed.; Plenum Press: New York, 1995.
(8) Ma, C.; Navrotsky, A. *Chem. Mater.* **2012,** *24*, 2311-2315.
(9) Birkner, N.; Navrotsky, A. *Am. Min.* **2012,** *97***,** 1291-1298.
(10) Schmalzried, H. *Pure Appl. Chem.* **2000**, *72*, 2137-2147.
(11) *Mineral–Water Interface Geochemistry, Reviews in Mineralogy and Geochemistry*; Hochella, M.F.; White, A.F., Eds; Mineralogical Society of America, 1990, vol. 23, p. 604.
(12) *Thermodynamics and kinetics of water rocks interaction, Reviews in Mineralogy and Geochemistry*; Oelkers, E.H.; Schott, J., Eds.; Mineralogical Society of America, 2009, vol. 70**,** p. 569.
(13) Nancollas, G.H. *Biological Mineralization and Demineralization*; Springer-Verlag: New York, 1982.
(14) Mann, S. *Biomineralization, Principles and Concepts in Bioinorganic Materials Chemistry*; Oxford University press: New York, 2002.
(15) *Biomineralization, Reviews in Mineralogy and Geochemistry*; Dove, P.M.; De Yoreo J.J.; Weiner, S., Eds.; Mineralogical Society of America, 2003, vol. 54**,** p. 381.
(16) Royer, M.L. *Bul. Soc. Franç. Minéral.,* **1928**, *51*, 7-159.
(17) van der Merwe, J.H. *Discuss. Faraday Soc.* **1949**, *5*, 201-214.
(18) Engel, O.G. *J. Res. N.B.S.,***1953**, *50*, 249.
(19) Becke, A.D. *J. Chem. Phys.* **1993**, *98*, 5648-5652.
(20) Lee, C.; Yang, W.; Parr, R.G. *Phys. Rev. B* **1998**, *37*, 785-789.
(21) Stephens, P.J.; Devlin, F.J.; Chabalowski, C.F.; Frisch, M.J. *J. Phys. Chem.* **1994**, *98*, 11623-11627.
(22) Bittarello, E.; Massaro, F.R.; Rubbo, M.; Costa, E.; Aquilano, D. *Cryst. Growth & Des.* **2009**, *9*, 971-977.

(23) Irving, D.L.; Sinnott, S.B.; Wood, R.F. *J. Phys.: Condens. Matter* **2004**, *16*, 4661-4676.
(24) Massaro, F.R.; Bruno, M.; Nestola, F. *Crystengcomm* **2014**, *16*, 9224-9235.
(25) Massaro, F.R.; Bruno, M.; Nestola, F. *Cryst. Growth & Des.* **2014**, *14*, 2357-2365.
(26) Bruno, M. *Crystal Research& Technology* **2013**,*48*, 811-818.
(27) Curie, P. *Journal de physique* **1894**, *3*, 393-415.
(28) Dovesi, R.; Civalleri, B.; Orlando, R.; Roetti, C.; Saunders, V.R. In: Reviews in Computational Chemistry; Lipkowitz, B.K.; Larter, R.; Cundari, T.R., Eds.; John Wiley & Sons, Inc.: New York, 2005, vol.1, p.443.
(29) Dovesi, R.; Orlando, R.; Civalleri, B.; Roetti, C.; Saunders, V.R.; Zicovich-Wilson, C.M. *Z. Kristallogr.* **2005**, *220*, 571-573.
(30) Dovesi, R. *et al.*, *CRYSTAL09 User's Manual*; University of Torino: Torino, Italy, 2009.
(31) Pisani, C.; Dovesi, R.; Roetti, C. *Hartree-Fock ab-initio treatment of crystalline systems*, Lecture Notes in Chemistry; Springer: Berlin, Heidelberg, New York, 1988.
(32) Bruno, M.; Massaro, F.R.; Prencipe, M.; Demichelis, R.; De La Pierre, M.; Nestola, F. *The Journal of Physical Chemistry C* **2014**, *118*, 2498-2506.
(33) Sobolev, N.V. *Deep-seated inclusions in kimberlites and the problem of the composition of the upper mantle*; American Geophysical Union: Washington, D.C., 1977.
(34) Orlov, Y.L. *The mineralogy of the diamond*; John Wiley & Sons: New York, 1977.
(35) Harris, J.W., Gurney, J.J. In: The properties of diamond; Field, J.E., Ed.; Academic Press: London, 1979, p. 674.
(36) Pearson, D.G., Shirey, S.B. In: Application of radiogenic isotopes to ore deposit research and exploration; Lambert, D.D.; Ruiz, J., Eds.; Society of Economic Geologists: Boulder, Colorado, 1999, vol. 12, p. 197.
(37) Nestola, F.; Nimis, P.; Anger, R.J.; Milani, S.; Bruno, M.; Prencipe, M.; Harris, J.W. *International Geology Review* **2014**, *56*, 1658-1667.
(38) Mitchell, R.S.; Giardini, A.A. *Am. Mineral.* **1953**, *38*, 136-138.
(39) De La Pierre, M.; Bruno, M.; Manfredotti, C.; Nestola, F.; Prencipe, M.; Manfredotti, C. *Molecular Physics* **2014**, *112*, 1030-1039.
(40) Hom, T.; Kiszenick, W.; Post B. *Journal of Applied Crystallography* **1975**, *8*, 457-458.
(41) Merli, M.; Oberti, R.; Caucia, F.; Ungaretti, L. *American Mineralogist* **2001**, *86*, 55-65.
(42) de Villiers, J.P.R. *American Mineralogist* **1971**, *56*, 758-766.
(43) Effenberger, H.; Zemann, J. *Zeitschrift für Kristallographie* **1979**, *150*, 133-138.
(44) Anderson, A.J.; Clark, A.H.; Gray, S. *Can. Mineral.* **2001**, *39*, 1513-1527.
(45) Rajam, S.; Mann, S. *J. Chem. Soc., Chem. Commun.* **1990**, 1789-1791.
(46) Nefyodova, I. V.; Lyutin, V. I.; Borodin, V. L.; Chvanski, P. P.; Leonyuk, N. I. *J. Cryst. Growth* **2000**, *211*, 458-460.
(47) Pastero, L., Costa, E.; Bruno, M.; Rubbo, M.; Sgualdino, G.; Aquilano, D. *Cryst. Growth & Des.* **2004**, *4*, 485-490.
(48) Massaro, F.R.; Pastero, L.; Costa, E.; Sgualdino, G.; Aquilano, D. *Cryst. Growth & Des.* **2008**, *8*, 2041-2046.
(49) Pastero, L.; Aquilano, D. *Cryst. Growth & Des.* **2008**, *8*, 3451-3460.
(50) Massaro, F.R.; Bruno, M.; Rubbo, M. *Crystengcomm* **2014**, *16*, 627-635.
(51) Aquilano, V; Rubbo, M.; Catti, M.; Pavese, A. *Journal of Crystal Growth* **1997**, *182*, 168-184.

For Table of Contents Use Only

A computational approach to the study of epitaxy: the natural occurrence in diamond/forsterite and aragonite/zabuyelite

Marco BRUNO,*[†] Marco RUBBO,[†] Linda PASTERO,[†] Francesco Roberto MASSARO,[†] Fabrizio NESTOLA,[‡] Dino AQUILANO[†]

[†] Dipartimento di Scienze della Terra, Università degli Studi di Torino, Via Valperga Caluso 35, I-10125, Torino Italy.

[‡] Dipartimento di Geoscienze, Università degli Studi di Padova, Via Gradenigo 6, I-35131, Padova Italy

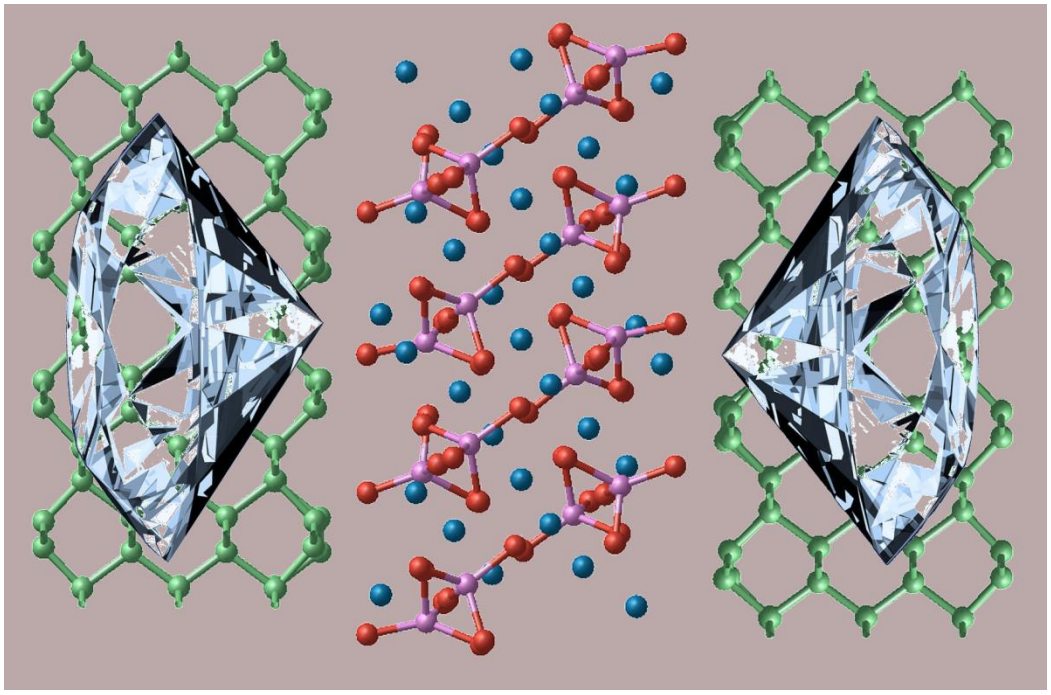

Synopsis

The theoretical and computational aspects concerning the epitaxy are discussed in a detailed way. The structure and adhesion energy of the {110}-diamond/{101}-forsterite and {001}-aragonite/{$\bar{1}$01}-zabuyelite interfaces were determined by means of *ab initio* calculations.